EFFECT OF CRYSTAL SIZE ON THE FAILURE MECHANICS OF POLYMER BONDED EXPLOSIVES

by

Chizoba Onwuka

Bachelor of Engineering
University of Nigeria, Nsukka, 2013

Master of Science
University of Ibadan, 2017

Submitted in Partial Fulfillment of the Requirements

For the Degree of Master of Science in

Mechanical Engineering

College of Engineering and Computing

University of South Carolina

2022

Accepted by:

Kidane Addis, Director of Thesis

Sutton Michael, Reader

Tracey L. Weldon, Interim Vice Provost and Dean of the Graduate School

DEDICATION

This Thesis is dedicated to almighty God for his grace and love for me. I would also thank my parents and my siblings for their support and encouragement in completing this research.

ACKNOWLEDGEMENTS

First and foremost, I would like to thank my advisor Dr. Addis Kidane, for his leadership, guidance, support and direction throughout my thesis. This research would not have been possible without his advice and encouragement. I also acknowledge Prof. Michael Sutton for his continuous support, insight, advice and valuable comments on my research throughout the duration of my master's degree program in University of South Carolina.

I would also love to extend my appreciation to the current and graduated DBMML research group members: Dr. Suraj Ravindran, Mr. Vijendra Gupta, Mr. Dennis Miller, Dr. Ali Fahem, Dr. Tessema Addis for their kind support, as well as Prof. Xiaomin Deng and Dr. Andrew Gross for their professional advice and support during my master's program.

My final appreciation goes to Lalitha Ravi, Renee Jenkins, Misty O' Donnel, Bill Bradly, for their kind assistance.

ABSTRACT

Polymer bonded explosives (PBXs), typically constitute 80-95% of energetic crystals and 5-20% of a soft polymer binder, are widely used in extreme loading conditions such as rocket propellants and explosive munitions because of their high performance and low sensitivity. The particle size of crystals has a significant effect on the mechanical properties of most polymer particulate composites.

In the study, the effect of particle size on the deformation behavior of PBX under dynamic loading is investigated. The study involves testing polymer bonded sugar (PBS) samples, a well-known mechanical simulant of PBXs, with four different crystal sizes: coarse, intermediate, fine and superfine with corresponding crystal sizes of 600-850 μm, 425-600 μm, 212-425 μm, and 100-212 μm, respectively. Dynamic compression load is applied to these samples using a split Hopkinson pressure bar (SHPB). The macroscale and local dynamic deformation of the samples are captured by taking series of images of the samples as it deforms using a high-speed camera.

From the macroscale experiment, it was observed that as the crystal size increase from superfine crystal size to coarse crystal size, the ultimate compressive stress of the PBS decreases. The mesoscale experiment shows that the local von Mises, axial and transverse strain fields of PBS for different crystal size specimens are different. The local strain fields in higher crystal size specimens such as coarse crystal size specimen are highly localized in the polymer rich regions, while more dispersed across the specimens with lower crystal size particularly superfine crystal size. The mechanism of

failure for different size crystal is discussed. This study would give an in-depth knowledge and understanding of how the crystal size affects the deformation mechanics of energetic and other particulate polymer composites.

TABLE OF CONTENTS

LIST OF TABLES

LIST OF FIGURES

CHAPTER 1

INTRODUCTION

1.1 BACKROUND

Polymer bonded explosives (PBXs) belong to a class of particulate composites that contains energetic crystals that adhere to a polymeric binder [1, 2, 3]. The energetic crystal is usually 75-96% of the total mass of the PBXs, while the remaining part constitute a small amount of polymer binder [4, 5]. The main function of the polymer binder is to desensitize the high explosive to unwanted external stimuli and provide a structural integrity to the composite material [6]. PBX may also contain additives such as plasticizers, oxidizers and antioxidants added in minute amounts to improve the performance of the explosive and decrease the effects of aging [7]. PBXs are used in a wide variety of applications particularly in military and civilian fields to develop products such as rocket propellants, weapons etc. [6, 8, 9,].

PBXs are highly heterogenous materials due to the presence of microscale voids, cracks and significant mismatch in the mechanical properties of the constituent materials [10]. During transportation, mechanical testing and storage, they can undergo loading at different timescales which may cause accidental detonation [5, 10]. It was observed that when PBX are impacted at a very low impact velocity, localized high temperature region called hotspots are formed which may cause explosion at a pressure below the threshold

shock [11, 12].This can pose a serious safety hazard and concern when they are handled or when they undergo mechanical testing. Hence, it is critical to understand the mechanical behavior of polymer bonded explosive when they undergo mechanical testing.

To characterize the mechanical behavior of PBXs with minimum safety requirements, it is ideal to utilize a mock PBX also known as simulant PBX. The reason is that a mock PBX can reproduce the mechanical behavior of a real PBX without the risk of detonation [13]. This would address the safety concern associated with the mechanical testing of PBXs.

In this study, the mechanical behavior of different crystal sizes of polymer bonded sugar – a mock explosive of PBXs -are investigated. Dynamic compression load is applied to the various crystal size specimens using a split Hopkinson pressure bar (SHPB). The macroscale and local dynamic deformation of the samples are studied and the global stress-strain curve for each crystal size as a function of strain rate is obtained and compared. Also, the full-field strain data is measured through 2D digital image correlation.

1.2 RESEARCH GOAL

A significant amount of research has been done in the past on polymer bonded explosives to understand their deformation and failure mechanisms. Studies done on PBXs include quasistatic [10] and dynamic [1-2, 4-5, 10, 14]. From Literature, it was discovered that the mechanical behavior of PBX depends on the size of the crystal of the explosive particle, and as the crystal size of the explosive increases, the strength of the

PBX decreases [14], this observation was mainly done from macroscale experiments. However, the macroscale experiments cannot provide adequate explanation to how the crystal size affects the strength of PBXs, this is because the global deformation behavior of particulate composites from macroscale experiments are controlled by the mesoscale [10].

The goal of this research is to study how the different crystal sizes of polymer bonded sugar affects the global and local deformation mechanisms of PBS at high strain rate loading.

Objectives of the thesis include:

1.) To compare the global stress-strain curve for each particle size as a function of strain rate

2.) To investigate the effect of particle size on the local deformation and failure mechanics of PBS.

This study would give an in-depth knowledge and understanding of how the crystal size affects the deformation mechanics of energetic and other particulate polymer composites.

1.3 THESIS STRUCTURE

This thesis is organized into five main chapters. The first chapter presents the introduction, background, research goal and objectives. The second chapter presents a literature review on studies conducted on polymer bonded explosives. The third chapter discusses the materials and methods used in the study. The fourth chapter present results and discussion from the study. The final chapter present conclusion and future work to be done to improve the applications of polymer bonded explosives.

CHAPTER 2

LITERATURE REVIEW

In this chapter, an overview of research work related to studies conducted on PBXs are done. This chapter discusses the use of split Hopkinson pressure bar and DIC technique to study the dynamic behavior of polymer bonded explosives.

2.1 DYNAMIC CHARACTERIZATION OF POLYMER BONDED EXPLOSIVES

Dynamic characterization is very vital in the study of polymer bonded explosives, this is because the mechanical response and damage mechanism of PBXs is heavily dependent on the loading method [10]. The main method used to study the damage behavior of polymer bonded explosives is the use of split Hopkinson pressure bar [15]. The apparatus is discussed extensively in [16, 17]. The dynamic performance behavior of polymer bonded explosives using split Hopkinson pressure bar have been extensively discussed [4-5, 10, 19, 20]. Parab et al. [18] observed that the cracking of HMX crystal particles under dynamic loading condition was caused by the tensile stress generated by the contacts between crystal particles.

Ravindran et al. found out that polymer bonded sugar (PBS) under dynamic loading does not exhibit significant strain hardening after yielding, however shows a long plateau region which is caused by the presence of polymeric binder [19]. Also, the global

deformation behavior of polymer bonded sugar is affected by the mass fraction of the individual constituent elements such that an increase in the mass fraction of the explosive particles causes the deformation behavior of PBS to shift from one being controlled by the polymeric binder to one controlled by the explosive particles [5].

Siviour et al. [20] utilized Split Hopkinson pressure bar to investigate the deformation of polymer bonded explosive -EDC 37- and they discovered that the deformation of EDC 37 depends on strain rates, with the strength increasing linearly with strain rate. Further, EDC 37 exhibits a clear yield point with conspicuous strain softening after yield. It was also discovered that PBX under dynamic loading behaves like a viscoelastic material and the binder affects the mechanical properties of PBX ,with the compressive strength increasing with binder content [2].

2.2 DIC A CONVENIENT METHOD TO STUDY THE LOCAL DEFORMATION OF PBS

There have been several techniques employed to study the deformation and mechanical properties at the surface of a material. Strain gauge is a useful technique used in the measurement of the average strain at a particular area on a material [21], however, this method has major limitations. First, it only provides the deformation at a single point [21]. Second, they are sensitive to overload and can damage easily when too much load is applied on them [22]. Finally, they are easily affected by temperature, fatigue and the measurement environment [23]. Hence it is not a convenient method to study the local deformation of a material as well as materials that have high impact load.

Alternatively, optical techniques, such as digital image correlation (DIC)- a non-contact measurement technique- can be used to study the full-field deformation in materials [24].

Many researchers have utilized DIC technique in experimental mechanics and have shown that the DIC method is a useful tool that can be widely used in the study of material deformation.[4-5, 10, 19, 25, 42]. Peters and Sutton et al. applied the idea of digital image correlation (DIC) to study the deformation of a material [25] and show that by comparing the same zone within digital images of the sample captured before and after deformation, the strain fields can be calculated.

Recently, authors have used digital image correlation (DIC) based experiments to measure the local strain deformation in PBX under dynamic loading [4-5, 10, 19]. They observed that a highly heterogenous local strain field was developed in PBX and the main failure mechanisms observed were de-bonding and crystal fracture [19]. Further, strain localization is dominant at the region filled with polymeric binder while the crystals either rotate or align themselves to accommodate the deformation in the binder [4]. In another work by same authors, it was discovered that shear banding in the material was caused by mechanical softening due to damage evolution and thermal softening in the material [19].

2.3 CONCEPT OF PARTICLE SIZE EFFECT ON THE DEFORMATION OF POLYMER BONDED EXPLOSIVES

The energetic particles and the matrix make up the components of polymer bonded explosives. However, the particles and the matrix combine to form the interphase with a characteristic length [26], if the mechanical properties of the interphase are different from those of the particles and the matrix, then the overall deformation of the

polymer bonded explosive will depend on the particle size. This is because for a fixed particle volume, the volumetric fraction of the interphase increases with a decrease in particle size [26]. Hence, the particle size is critical in the deformation behavior of polymer bonded explosives.

Several researchers have studied the effect of particle size on the deformation of PBXs. Siviour CR et al. found out that increasing the crystal size of the explosive decreases the strength of PBX [14], since the average number of inter-particle contact is inversely proportional to the stresses arising between the particles [27]. Kumar KR, et al. investigated the effect of aluminum particle size on the compressive stress-strain behaviors of aluminum composite using split Hopkinson pressure bar at intermediate strain rate (1550/s) and found out that the strength increased with decreasing aluminum particle size. The smaller particle size showed a rise to peak stress followed by a slight strain softening while the bigger particle size showed a rise to peak stress followed by a rapid fall in strength [28].

Shao-Yun F, et al. found out that for a given particulate volume fraction, as the particle size decreases, the strength of the composite increases because smaller particles have higher total surface area for a given particle loading which enables a more efficient stress transfer mechanism [29].

Matthew JH, et al. utilized a PBX surrogate 5-iodo-2′-deoxyuridine (IDOX) for the explosive cyclotetramethylene-tetranitramine (HMX) to investigate the effect of IDOX particle size distribution on the compressive strength by uniaxial compressive testing. It was discovered that the contacting crystal carries most of the force, the smaller

crystals are less likely to crack or slip during compressive loading thus resulting in a stronger composite than their larger particle size because their crystals pack closely to each other [30]. The larger crystals on the other hand, has loose or poor crystal packing, when loaded, crystal breakage easily occur, which could cause weakening of the material [31, 32].

Kezhen L V et al. investigated the effect of particle size on the strength of polymer bonded explosive using ultrasonic vibration loading and found out that the strength increases with decrease in particle size. The reason is because of particle contact in PBX. The smaller particle size has higher specific surface area than the higher particle size. Consequently, having more particle contact. Further, the smaller particle size would lead to higher binder area, which results to higher bonding strength, which is also the reason for the strength increase [33]

Balzer J. E. et al. studied the dynamic behavior of 3 ammonium perchlorate-based propellants(CPX 372) explosive using a split Hopkinson pressure bar and found out that small particles comprising of AP (3-300μm) deformed at higher stress compared to larger particles (200-300μm). Also, strain hardening was more pronounced for smaller particle size materials. It was also discovered that the flow stress was indirectly proportional to the square root of the grain size [34], and [35] studied the damage behavior of 3 RDX-HTPB explosives of different particle size- coarse, fine, mix of coarse and fine- and discovered that composites containing coarse particles suffered more severe damage and have lower strength than the fine particle size.

CHAPTER 3

MATERIALS AND METHODS

3.1 CONSTITUENT MATERIALS

The manufacturing process of polymer bonded sugar (PBS) is complex; hence it is very important that appropriate materials are selected when producing PBS. The reason is that the specific mechanical behavior of each constituent materials of PBS contribute significantly to the mechanical behavior of the resulting mock explosive. Hence material selection is critical in the manufacturing process of PBS. The following materials are used in the production of polymer bonded sugar, and they are shown in figure 3.1(a)-(d).

Polymeric binder: The polymeric binder which provide a structural integrity to the polymer bonded explosive [6] is prepared from a combination of hydroxyl terminated polybutadiene (HTPB), di-octyl sebacate (DOS) and toluene diisocyanate (TDI). The constituent materials used in the preparation of the polymeric binder are discussed as below.

Hydroxyl terminated polybutadiene (HTPB): HTPB is the binder used to manufacture polymer bonded sugar used in the study. It is gotten as a free sample from RCS Rocket Motor Components USA, and it is shown in figure 3.1 (a). HTPB is a colorless viscous liquid that belongs to the class of polyurethane binders that is widely used in propellants and explosive industries due to its good mechanical, hydrolytic stability and aging

properties [36]. It's glass transition temperature T_g and density are -75°C , and 916 kg/m^3 respectively [37].

Toluene diisocyanate (TDI): Toluene Diisocyanate(TDI) as shown in figure 3.1 (b) is a colorless liquid with a sharp pungent odor used in the production of polyurethane binders [38]. It is used in PBS as a curing agent by crosslinking of polymer chains of the polymeric binder. It was purchased from Sigma-Aldrich, USA.

Di-octyl sebacate (DOS): Dioctyl sebacate also known as di(2-ethylhexyl) sebacate shown in figure 3.1 (c) is a colorless liquid used as a plasticizer in the production of PBS. It is used to lower the glass transition temperature T_g of the binder [39] . It was purchased from Sigma-Aldrich, USA.

Simulant Energetic Particle (Sugar crystals): The energetic particle used for the study is raw cane sugar crystals that range between 100-850μm as shown in figure 3.1 (d). It was produced by Florida crystals corporation and purchased from Amazon company USA. Even though sugar is far from representing the actual microstructure of well popular explosives such as RDX and HMX, sugar was selected as the simulant energetic particle because of the following reasons.

First, the deformation behavior of polymer bonded sugar macroscopically is similar to most polymer bonded explosives [40]. Further, the monoclinic structure of sugar is like the monoclinic crystalline structure of high melting point explosives [41] and finally, sugar is a non-hazardous substance which makes it a convenient surrogate for the explosive material to be tested in university laboratories and facilities[10].

3.2 EQUIPMENT

Scale: E01140 Ohaus explorer analytical balance scale with capacity of 110g and accuracy of 0.0001 g.

Hydraulic Press: MTS Hydraulic Actuator. Model Number 318.25, Serial number: 0239425 With a force capacity of 250KN.

Oven: Thermo scientific precision oven with model number 6528 and S/N:600894 with temperature range 65°C -200°C and sensitivity ± 0.5°C.

Sieves: 4 sets of standard testing sieves made by Endecott's with aperture of: 850 μm, 600 μm, 425 μm and 212 μm.

Containers, measuring cups and stirring rods: Sets of deli containers, graduated measuring cups and plastic stirring rods was used during the mixing processes of PBS.

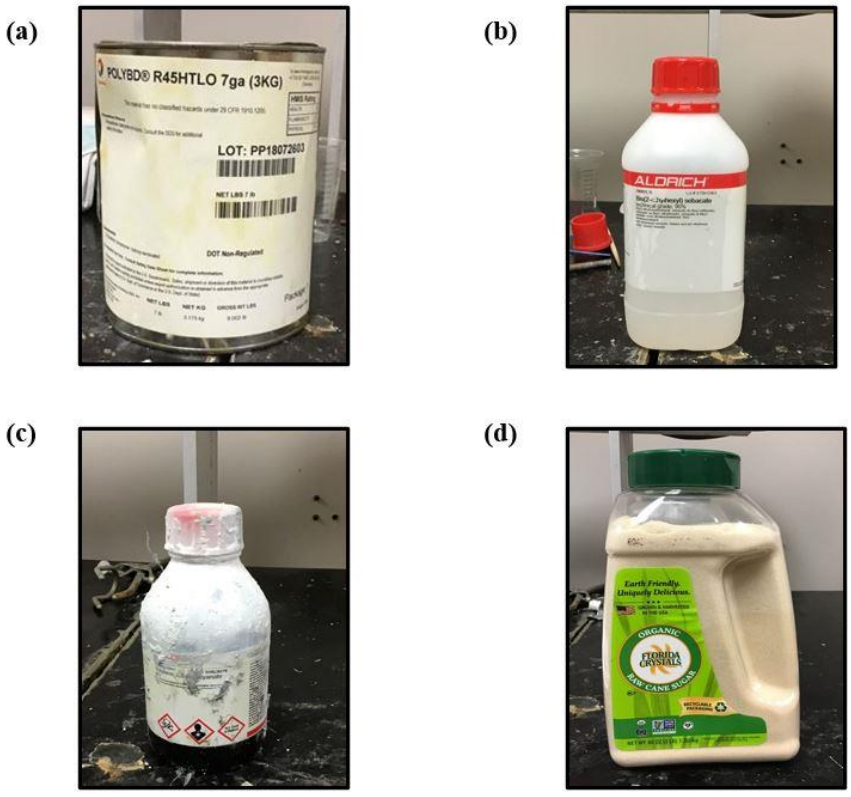

Figure 3.1 (a) Hydroxyl terminated polybutadiene (HTPB) (b) Toluene diisocyanate (TDI) (c) Di-octyl sebacate (DOS) (d) Simulant Energetic Particle(Sugar crystals)

3.3 MANUFACTURING METHOD

The detail sample preparation involves 3 steps, and they are discussed as follows. Separating of sugar into different crystal sizes: The purchased sugar is separated into different crystal sizes: coarse, intermediate, fine and superfine using a sieve of size 850μm, 600μm, 425μm and 212μm respectively as shown in figure 3.2 (a). After the sugars are separated into different crystal sizes, they are poured inside a container and labelled accordingly as shown in figure 3.2 (b).

(a)

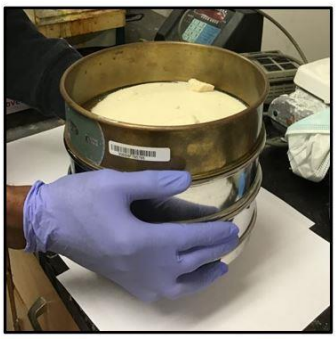

(b)

Figure 3.2 (a) Sugar crystals inside sieves of different sizes (b) Different crystal sizes of sugar

Mixing of constituent materials: Hydroxyl terminated polybutadiene (HTPB) was mixed with di-octyl sebacate DOS (Plasticizer) and toluene diisocynate TDI (curing agent) in a specified ratio as shown in Table 3.1 to obtain plasticized HTPB solution as seen in figure 3.3(a). Thereafter, the solution is added to the individual sugar crystal sizes obtained earlier and mixed thoroughly for about 15-20 minutes to coat the surface of the sugar crystals with the polymeric binder as shown in figure 3.3(b). Then, the resulting mixture was kept in an oven for about 4 hours at 80°C. This process is regarded as partial curing and it helps in enhancing the binding properties of the coated polymers.

Table 3.1 Compositions of different crystal size samples

Type	Crystal size (μm)	Sugar (% wt.)	HTPB (% wt.)	DOS (% wt.)	TDI (% wt.)
Coarse	600-850	95.00	3.60	0.96	0.44
Intermediate	425-600	95.00	3.60	0.96	0.44
Fine	212-425	95.00	3.60	0.96	0.44
Superfine	100-200	95.00	3.60	0.96	0.44

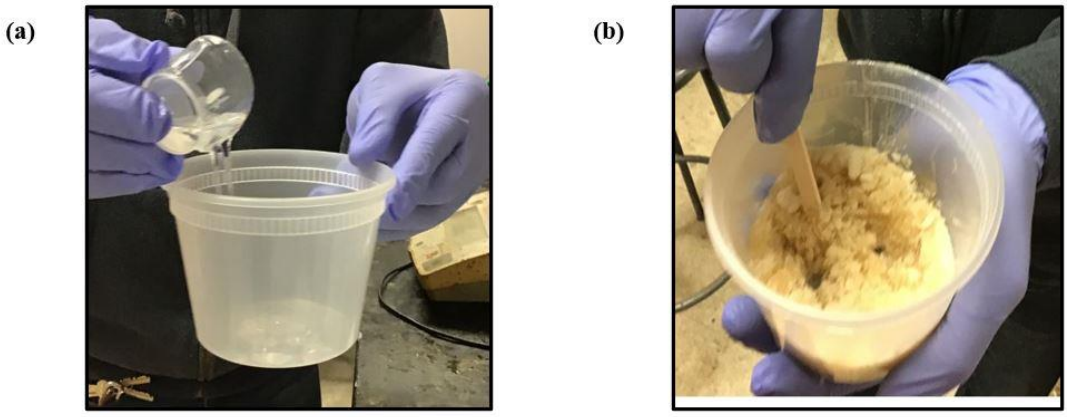

Figure 3.3 (a) HTPB being poured inside a container (b) mixing of constituent materials.

Pressing and machining of the sample

The partially cured mixture obtained was pressed at 90 MPa in a steel mold of 25.4mm diameter shown in figure 3.4(a) at room temperature using MTS machine as shown in figure 3.4(b) to produce sets of polymer bonded sugar samples of circular cross-section as seen in figure 3.4(d). After the samples are produced, they are placed in an oven

at 80°C for 48 hours to completely cure the samples. Finally, the cured samples were machined to form a cube geometry of side 14mm using a milling machine as shown in figure 3.5(a) to facilitate 2D digital image correlation. The specimen dimensions as well as the real image of the specimen are shown in figure 3.5(c) and (d) respectively.

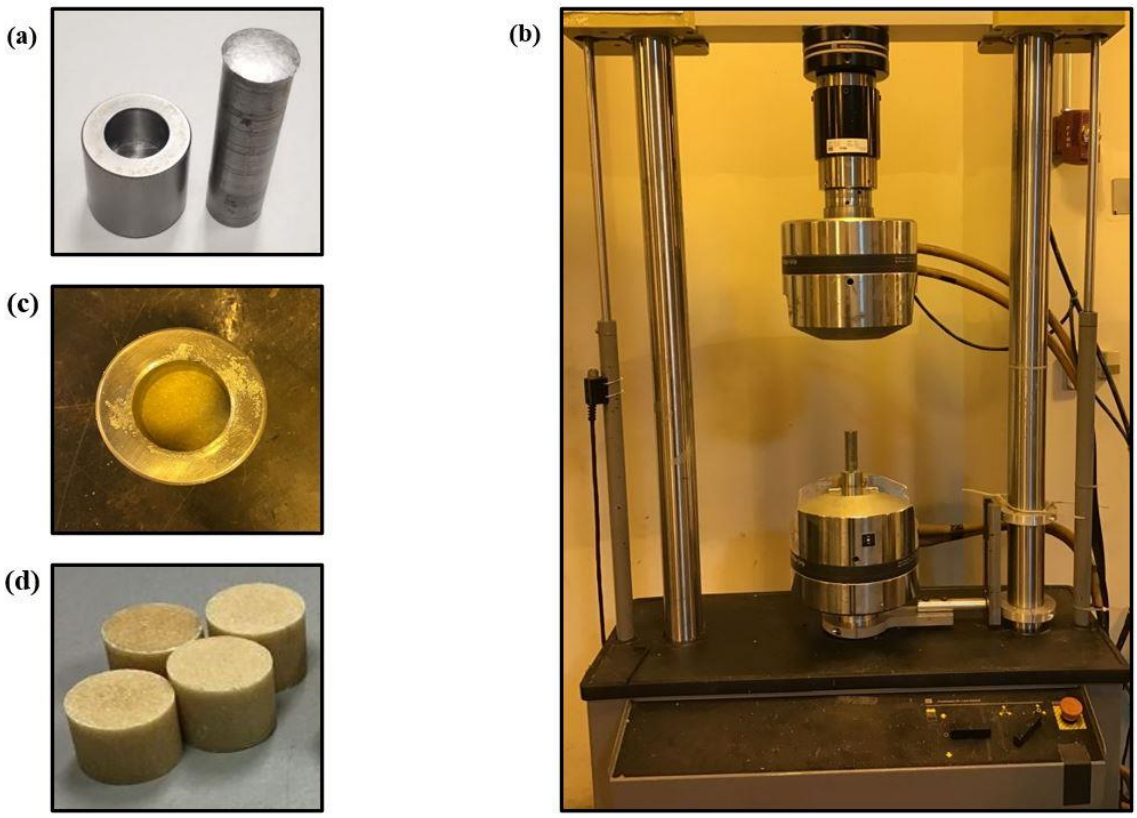

Figure 3.4 (a) Steel mold of (b) The specimen set to be compressed by the MTS machine (c) Specimen after being compressed (d) Set of polymers bonded explosive samples

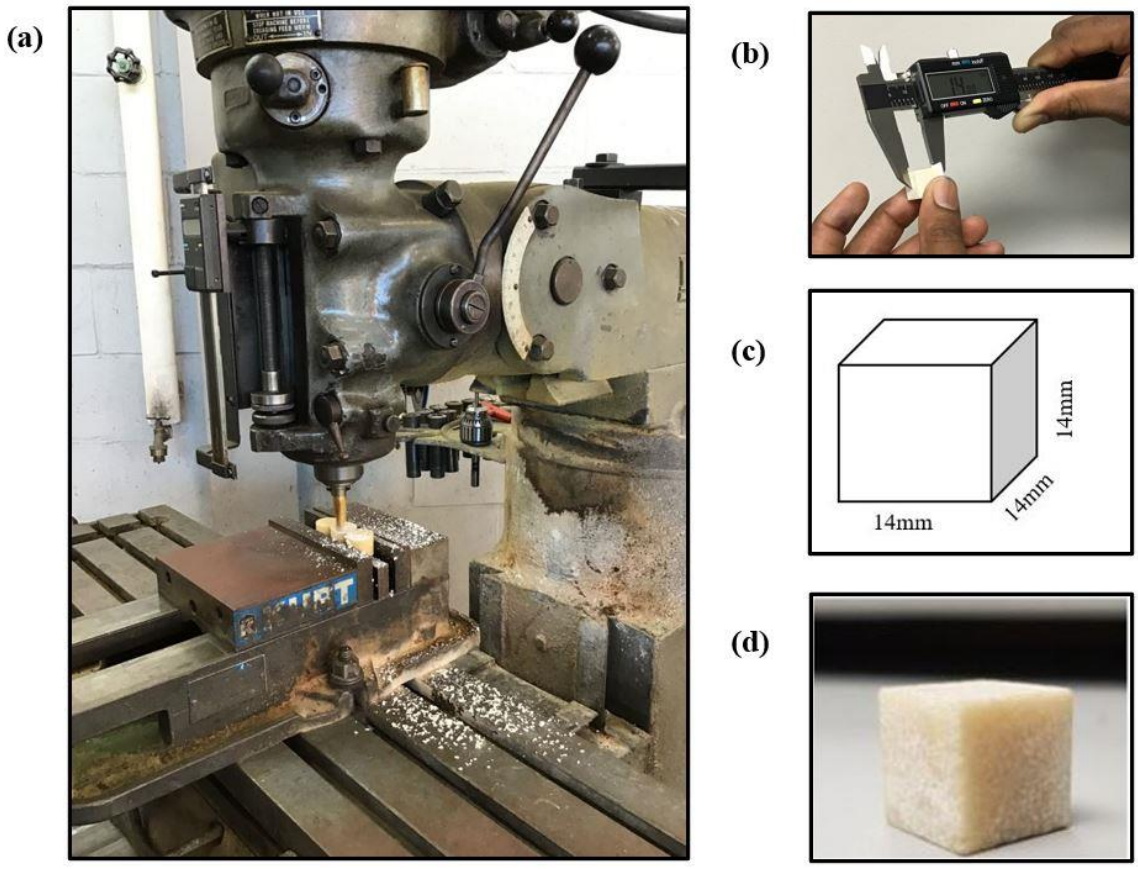

Figure 3.5 (a) Specimen being machined by vertical milling machine (b) The specimen being measured with a caliper (c) Dimension of the specimen (d) polymers bonded explosive sample.

3.4 SURFACE PREPARATION FOR MACRO AND MESOSCALE DIGITAL IMAGE CORRELATION (DIC)

To enhance DIC measurement, two different methods of speckling were adopted for the macroscale and mesoscale experiments respectively. For the macroscale experiment, a high contrast, random and isotropic speckle is applied on the surface of the specimen. Detail process of choosing the right speckle can be seen in [42]. To apply speckles on the surface of the specimen, first, the specimen is clamped vertically on a tripod stand and a thin coat of white paint was applied to the surface of the specimen followed by a black paint. The selected speckle size is between 500-600 μm. The

specimen dimensions with speckle pattern for the macroscale DIC measurement and the actual image of the specimen after speckling are shown in figure 3.6(a) and 3.6(b) respectively.

For the mesoscale digital image correlation, three major steps are followed- polishing, marking and speckling to relate the strain fields at grain scale level with the underlying microstructure. The processes are discussed below.

First, the specimen was dry polished with silicon carbide paper of grid size of 800-1200μm attached to a polishing machine as shown in figure 3.6 (c).

Second, the area of interest (AOI) on the specimen was marked using a HB pencil. Thereafter, the left and top part of the specimen is covered with a scotch tape as L shape leaving the microstructure of the right bottom side of the specimen for imaging and speckling. To facilitate easy matching of the strain contour plots with the underlying microstructure, an ultra-high-speed imaging camera HPVX2 by Shimadzu was used to take the microstructure images of the sample. Details of this camera is discussed in section 3.5.

Finally, The AOI is speckled, to speckle the specimen, a white paint was applied on the specimen using an air brush and a black toner powder is deposited immediately on the partially dried white paint using an air gun and allowed to dry completely, Thereafter, the scotch tape was removed to give an average speckle size of 20-40μm. A schematic diagram of the sample showing the speckle patterns of AOI is shown in figure 3.6 (d).

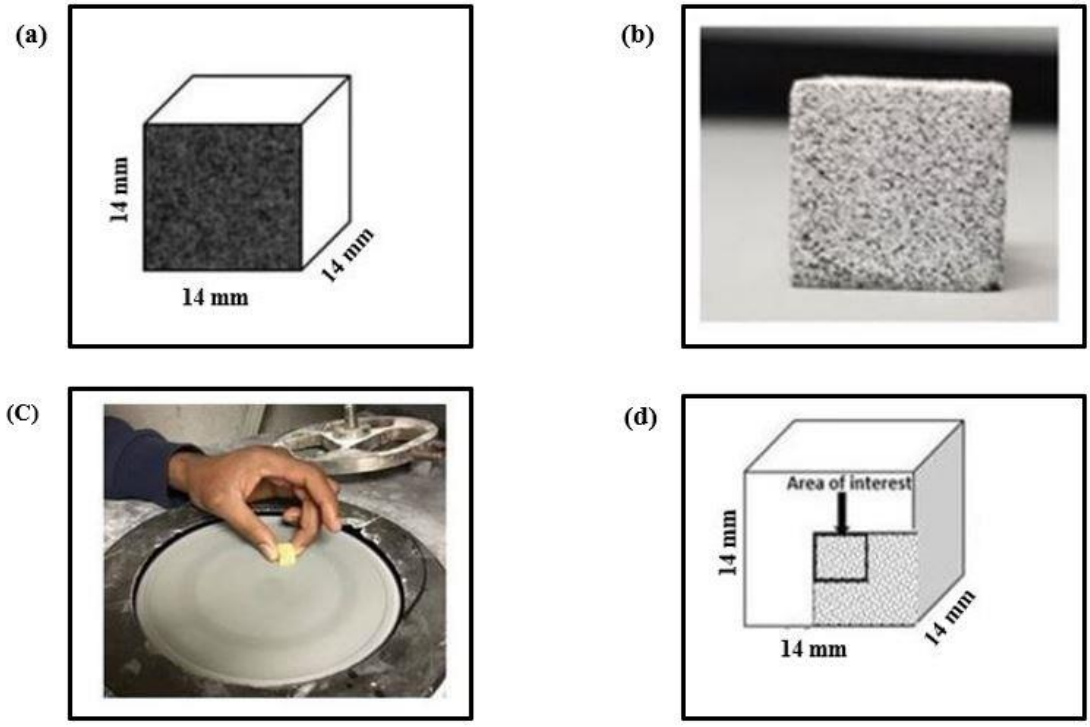

Figure 3.6 (a) Dimension of the specimen for macroscale experiment (b) Original Image of the specimen for macroscale experiment (c) Specimen being polished with a carbide paper (d) Specimen dimension for the mesoscale experiment with AOI=4.28mm x 2.40mm.

3.5 EXPERIMENTAL SETUP AND DATA ANALYSIS

The specimen was dynamically compressed via a split Hopkinson pressure bar (SHPB) setup consisting of an incident and a transmitter bar of length and diameter of 1830 mm and 25.4 mm, respectively. The schematic description and the actual photograph of the experimental setup are shown in figure 3.7(a) and (b) respectively. To reduce friction between the bars and the specimen, a thin layer of grease is applied gently at the interface between the bar and the specimen. Since the specimen is made of low impedance material, polymeric bars are used as the incident and transmitter bars to prevent impedance mismatch between the specimen and the bars [43]. Thereafter, the

strains in the bars are measured with the help of the strain gauges attached at the middle of the incident and transmitter bars, and used to calculate the average strain rate, strain, and stress in the specimen using equation 1 to 3 below.

Specimen strain rate; $\dot{\varepsilon}_s(t) = \frac{-2C_b}{l_s}\varepsilon_{r(t)}$ (1)

Strain in the specimen; $\varepsilon_s(t) = \int_0^t \frac{-2C_b}{l_s}\varepsilon_{r(t)}dt$ (2)

Stress in the specimen; $\sigma_s(t) = \frac{E_b A_b}{A_s}\varepsilon_{t(t)}$ (3)

where 'l_s' is the length of the specimen, '$\varepsilon_{r(t)}$' is the reflected strain signal. '$\varepsilon_{t(t)}$' is the transmitted strain signal. C_b = 1470 m/s' is the speed of the wave in the polymeric bar, and 'E_b= 2.5 GPa' is the modulus of Elasticity of the bar material. 'A_b ' is the cross-sectional area of the bar, and 'A_s' is the cross-sectional area of the specimen.

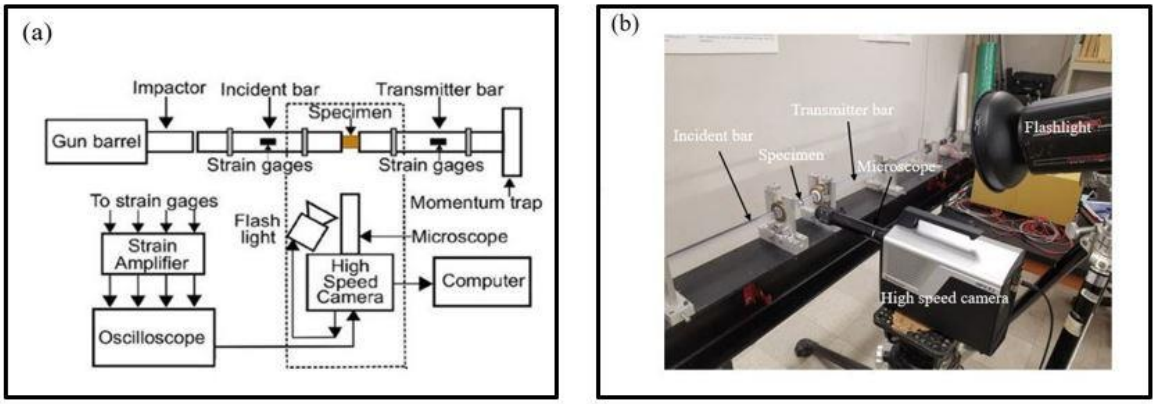

Figure 3.7 (a) Schematic description of the experimental setup. Diagram was extracted from [5] (b) The actual image of the experimental setup.

To measure the macroscale and mesoscale full-field strain using DIC, an ultra-high-speed imaging camera HPVX2 by Shimadzu was used. The camera has the capability of capturing 10 million images per second, however, the image acquiring rate selected for the study are 100,000 frames/seconds and 1,000,000 frames/seconds for the macroscale and mesoscale experiments and it was able to capture the total duration of the dynamic events. For the macroscale experiment, a 100mm Tokina lens that yielded a field of view of 27.2mm x 17.0mm at a resolution of 100 μm/px was used, while for the mesoscale experiment, a high magnification far field microscope was attached to the camera. The high magnification microscope yielded a field of view of 4.28 x 2.40mm at a resolution of 10.73 μm/px . Since high illumination is needed for dynamic experiments at high frame rate, a photogenic flash lamp was used to illuminate the sample.

The images acquired during the experiment were post-processed in VIC-2D, a commercial software by correlated solutions. A subset size of 21 x 21 and 9 x 9 were used for the macroscale and mesoscale experiments respectively which considers at least 3x 3 speckles in a subset. The step size and filter size selected for the macroscale experiment were 4 pixels and 15 respectively while a step size of 2 pixels where chosen for coarse, intermediate and fine crystal size specimens and 1 pixel for superfine crystal size for the mesoscale experiment. A filter size of 9 were chosen for all the crystal size specimens for the mesoscale experiments. The matching algorithm chosen for both the macroscale and mesoscale experiment is zero normalized squared difference(ZNSD). To convert the digital signal into continuous data, an optimized 8 tap interpolation function was selected. Complete information of the imaging and postprocessing parameters for

both the macroscale and mesoscale experiments can be seen in Table 3.2 and Table 3.3 respectively.

Table 3.2 Image parameters used in the study

Parameter	Macroscale	Mesoscale
Imaging Lens	100 mm Tokina Lens	Navitar extension tube
Field of view	27.20 mm x 17.00mm	4.28mm x 2.40mm
Imaging frame rate	100,000fps	1,000,000fps
Pixel to length ratio	100.00 μm/px	10.73 μm/px

Table 3.3 Post processing parameters used in the study.

Parameter	Macroscale	Mesoscale
Correlation criteria	ZNSD	ZNSD
Interpolation	Optimized 8-tap	Optimized 8-tap
Subset size	21 x 21 pixel^2	9 x 9 pixel^2
Step size	4 pixels	Superfine crystal size specimen= 1pixel other crystal size specimens= 2 pixels
Filter size	15	9

CHAPTER 4

RESULT AND DISCUSSION

4.1 MACROSCALE DEFORMATION BEHAVIOR

Figure 4.1(a)-(d) shows the voltage time signal recorded from the oscilloscope for coarse, intermediate, fine and superfine crystal size specimens. The blue and yellow curves are the incident and reflected waves voltages recorded by the strain gage on the incident bar while the purple and green curves are the transmitted wave voltages recorded by the strain gage on the transmitter bar. The amplitude of the incident wave and transmitter wave voltage are negative indicating compression while the amplitude of the reflected wave voltage is positive indicating tension. The voltages are further plotted on the same scale as shown in figure 4.2 (a)-(d).

The voltages from the oscilloscope are further converted to strains following steps outlined in [44]. These strains calculated based on the measured data from the strain gage are compared with strains obtained from 2D DIC for coarse crystal size specimen as shown in figure 4.3. The strains from 2D DIC and strain gage are nearly equal, although there are some slight variations between them especially during the latter time of deformation which could be due to error introduced in DIC when failure start occurring in the material.

To verify force equilibrium in the sample when it is loaded. The forces on the left and right part of the specimen known as the incident force F_i and transmitter force F_t respectively as seen in figure 4.4(b) are measured and shown in figure 4.4(a). These two forces even though showed some discrepancy during the early stage of loading, are nearly equal later indicating that equilibrium is achieved in the sample.

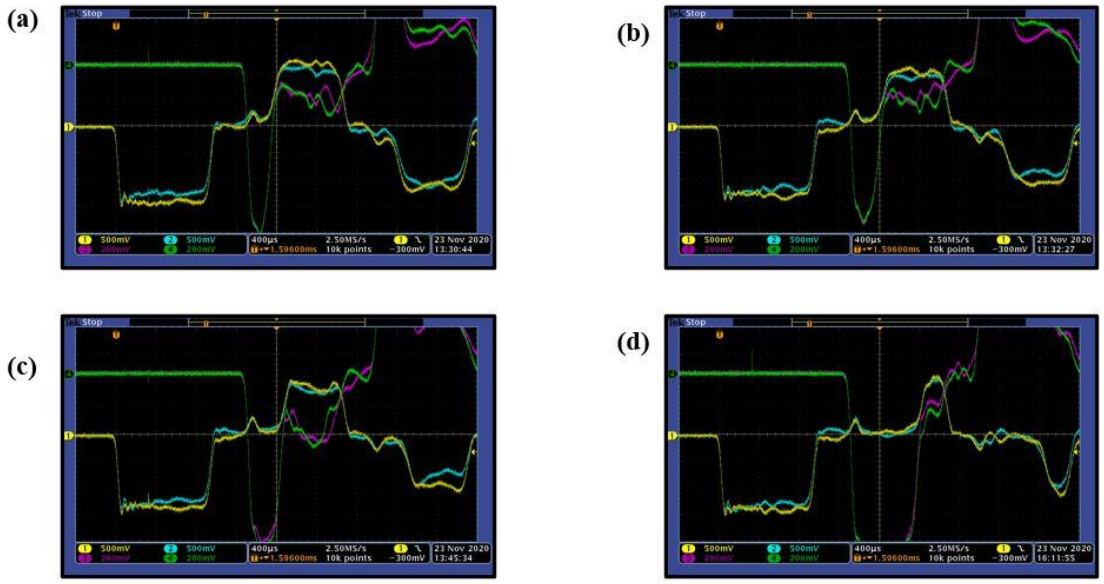

Figure 4.1 Voltage vs time signal obtained from oscilloscope for (a) coarse crystal size (b) intermediate crystal size(c) fine crystal size (d) Superfine crystal size

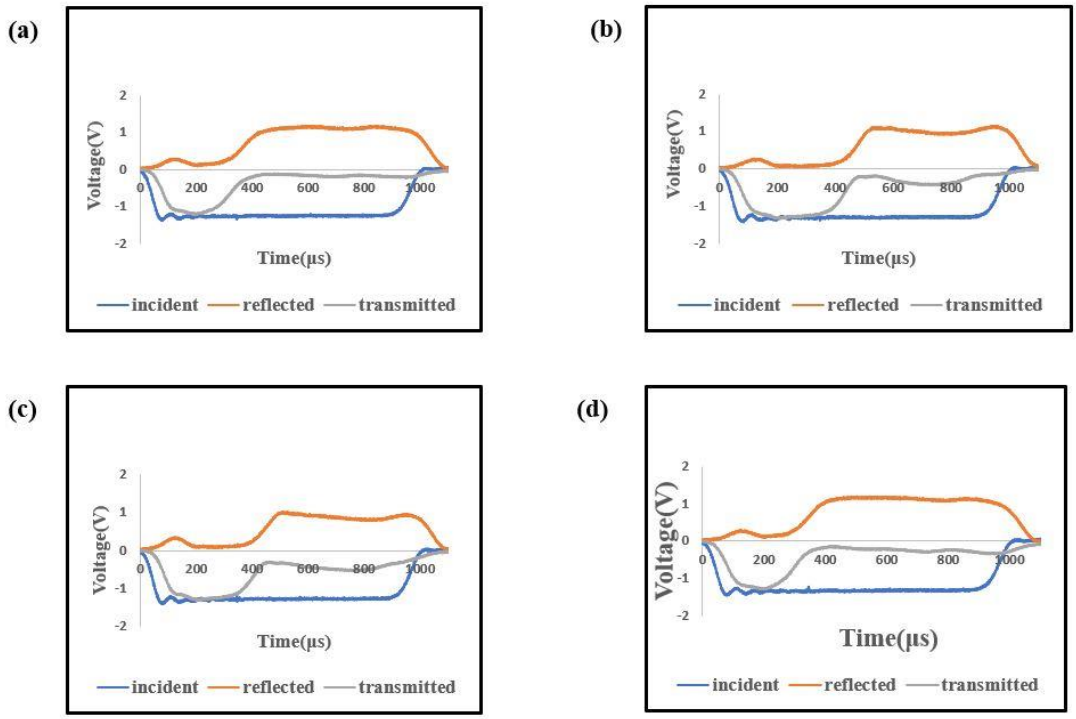

Figure 4.2 The incident, reflected and transmitted signal (a) coarse Particle size(b) intermediate Particle size(c) fine particle size (d) Superfine Particle size

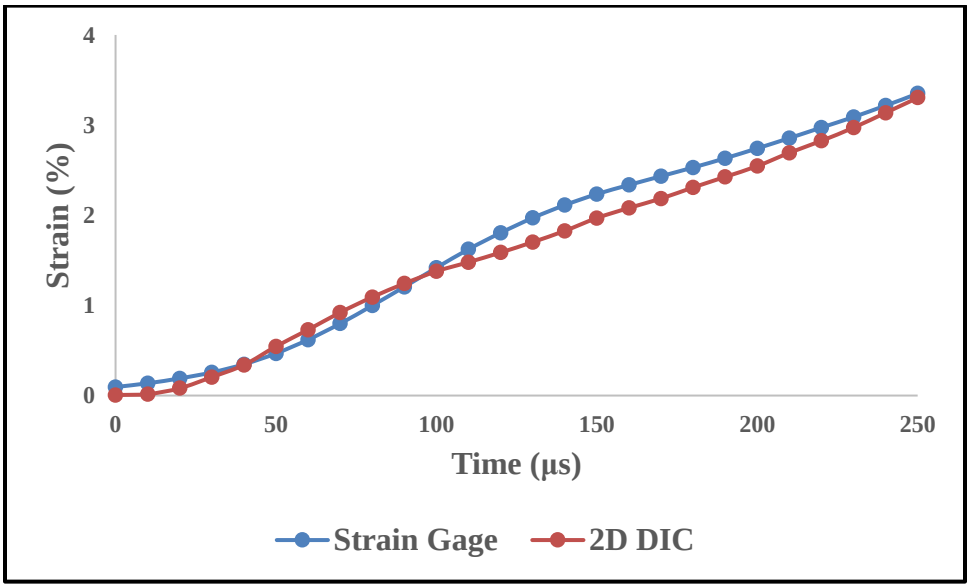

Figure 4.3 Comparison of DIC strain measurement with the strain gage measurement figure shows the strain versus time for coarse particle size specimen

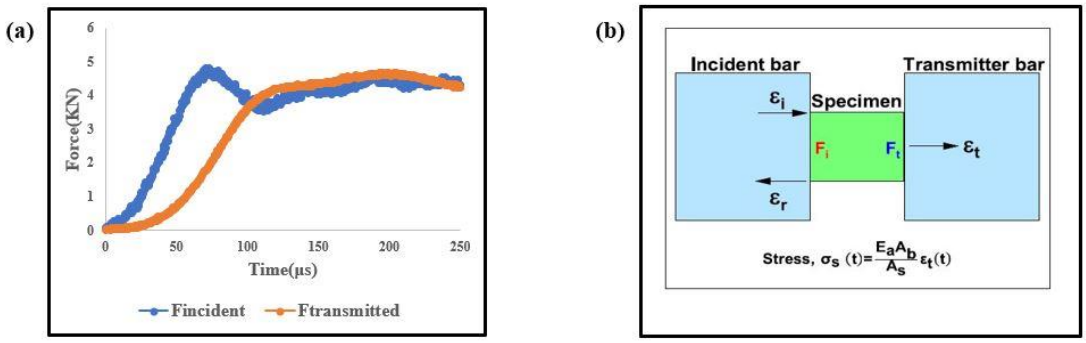

Figure 4.4 (a) force versus time at incident and transmitter side of the bars (b) Diagram showing specimen sandwiched between the incident and transmitter bar, extracted from [19]

The image captured during the deformation of the sample for coarse, intermediate, fine and superfine crystal size specimens are shown in figure 4.5-4.8 respectively. Fracture started occurring for the coarse crystal size as early as about 290μs, 330μs and 400μs for intermediate and fine particle size specimens respectively and much later, about 690μs for the superfine crystal size. The average axial strain vs time is plotted for all the crystal size specimens in figure 4.9. It was found out that fracture started to occur at about 3.55% average strain for the coarse crystal size, 2.87% for the intermediate, (for fine crystal size, the image went out of focus, and it is difficult to determine when fracture started) and 2.55% for the superfine crystal specimens size respectively.

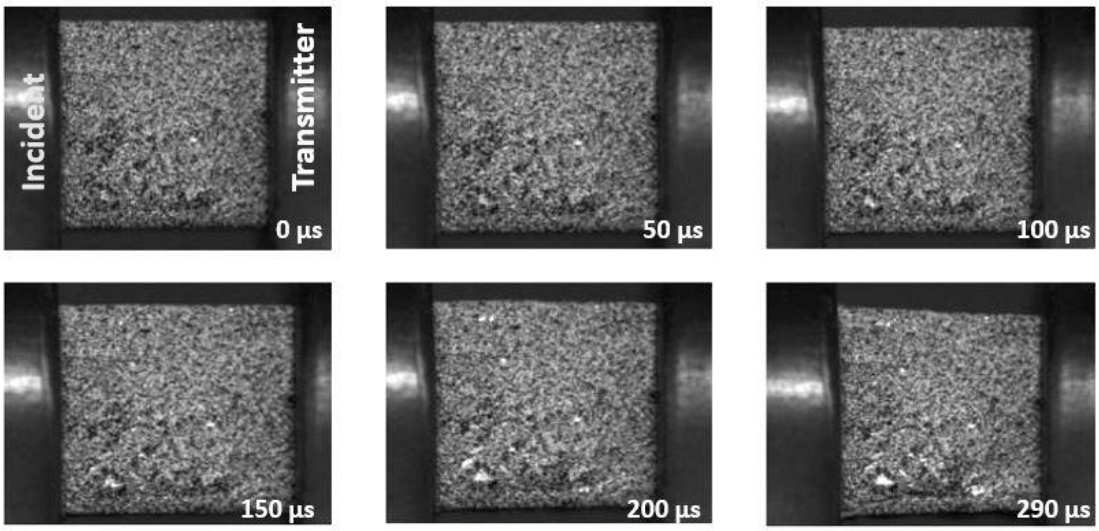

Figure 4.5 Raw images of coarse crystal size specimen during deformation

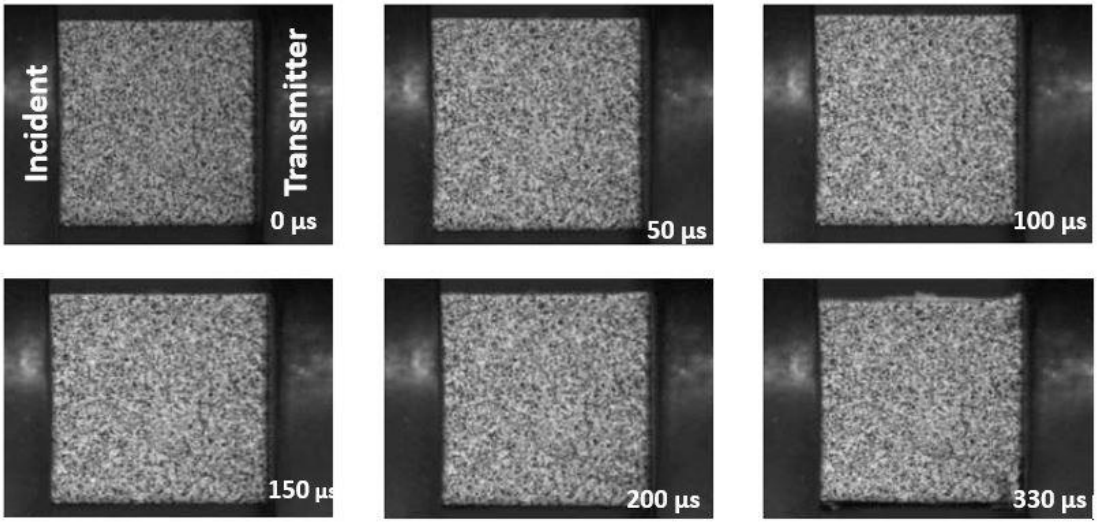

Figure 4.6 Raw images of intermediate crystal size specimen during deformation

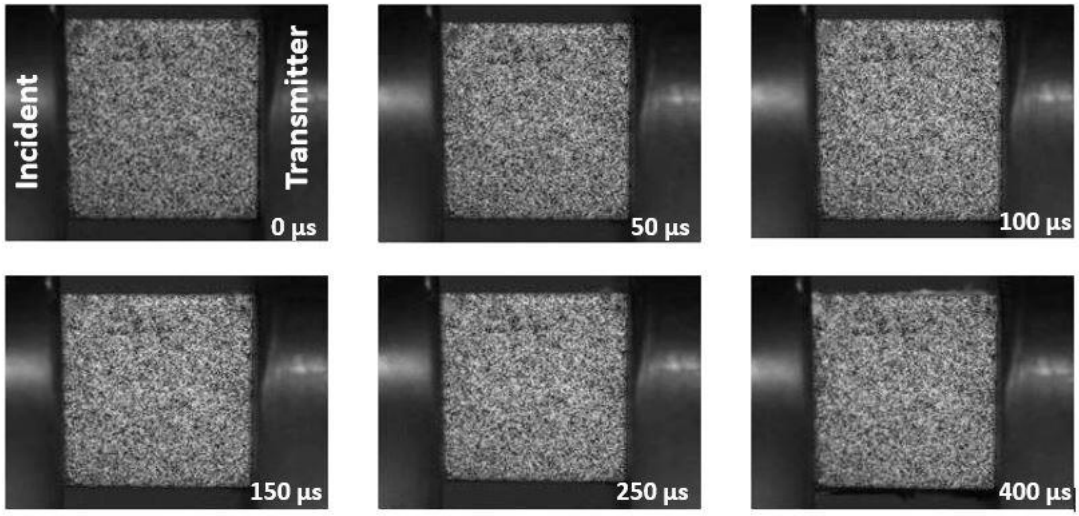

Figure 4.7 Raw images of fine crystal size specimen during deformation

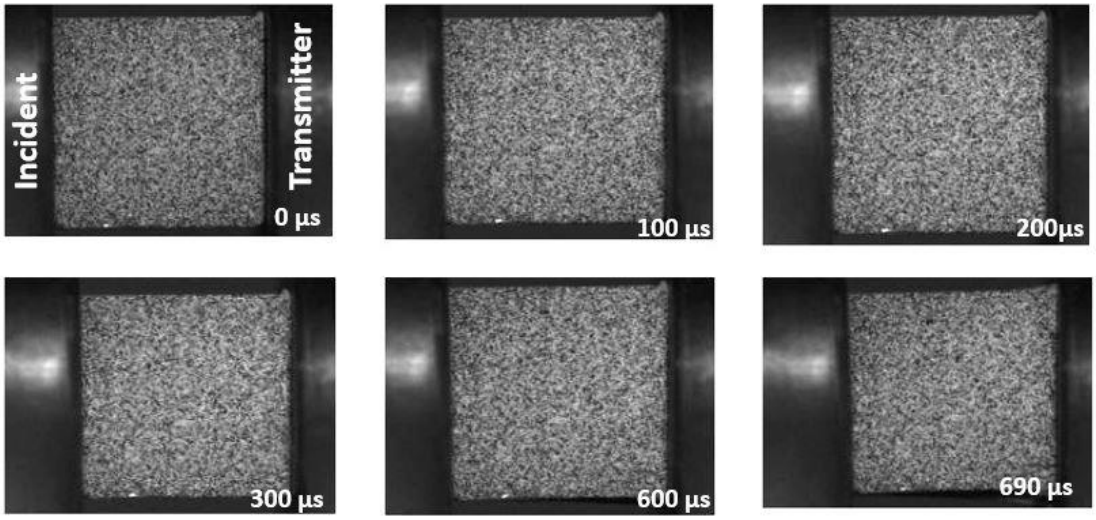

Figure 4.8 Raw images of super fine crystal size specimen during deformation

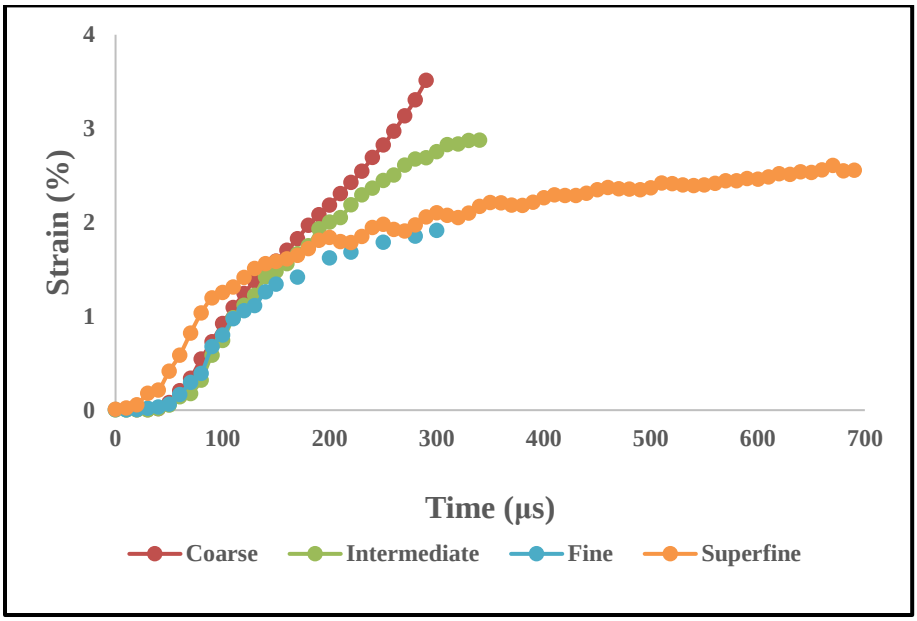

Figure 4.9 The axial strain vs time for coarse, intermediate, fine, and superfine crystal size specimen.

Fig. 4.10 shows the global stress-strain curves for coarse, intermediate, fine and superfine crystal size specimens of polymer bonded sugar. The coarse crystal size specimen corresponding to 600-850µm crystal size reached an ultimate compressive stress of 23.61MPa at around 2.18% global axial strain while the ultimate compressive stress and corresponding strain of the superfine crystal size specimen corresponding to 100-212µm crystal size are 27.00MPa and 1.72% respectively. The ultimate compressive stress and the corresponding strains for the remaining crystal size specimens are shown in Table 4.1.

Table 4.1 The ultimate compressive stress and its corresponding strain for different crystal sizes of PBS

Type	Crystal Size (μm)	Avg. Density (g/cm^3)	Ultimate Compressive Stress (MPa)	Strain (%)
Coarse	600-850	1.44	23.61	2.18
Intermediate	425-600	1.44	24.47	1.71
Fine	212-425	1.47	25.58	1.68
Superfine	100-200	1.52	27.00	1.72

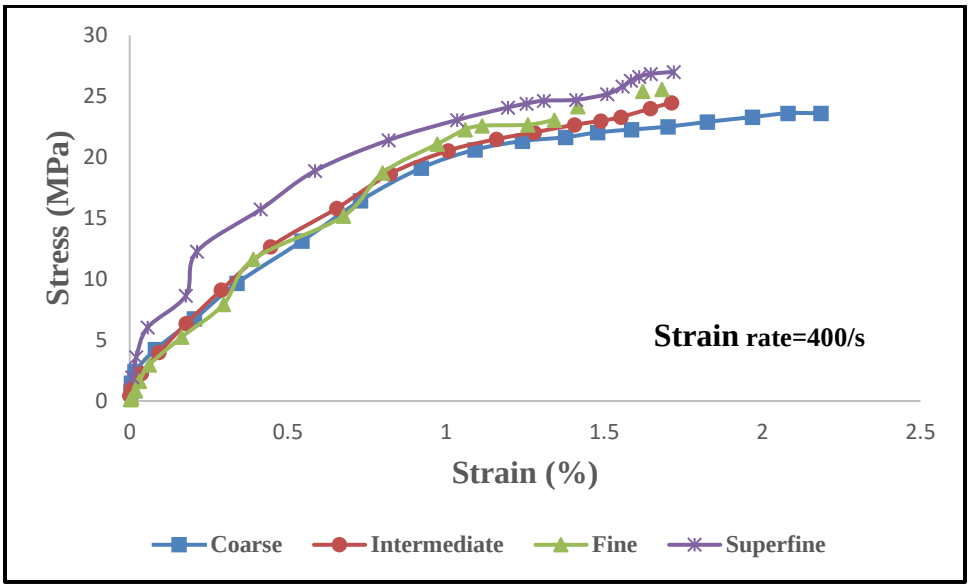

Figure 4.10 Global Stress-strain curves for different crystal sizes of polymer bonded sugar

From the result, it was observed that as the crystal size increase from superfine crystal size to coarse crystal size, the ultimate compressive stress of the PBS decreases. A similar behavior was observed for RF 38-22 (159 μm) and RF 38-09 (710 μm), polymer bonded explosives prepared with a mixture of cyclotrimethylene trinitramine (RDX) hydroxyl-terminated polybutadiene (HTPB) binder where the higher crystal size deforms at a lower stress than the lower crystal size [7].

To explain this phenomenon, the average number of interparticle contacts is considered. Accordingly, superfine crystal size has higher ultimate compressive stress than coarse crystal size and this could be due to the average number of inter-particle contacts are higher in superfine crystal size specimen than in coarse crystal size specimen. A high number of contacts between the crystals, would enhance interparticle interactions and reduce the average stress between the particles [7]. Since high inter-particle contacts correspond inversely to the stresses arising between the particles [27]. Thus, the specimen corresponding to superfine crystal size would have a higher ultimate compressive stress. Similarly, coarse crystal size with lower average number of contacts would crush at lower axial load. A similar trend is also observed for intermediate and fine crystal size specimens.

4.2 MESOSCALE DEFORMATION BEHAVIOR

Distortion correction is unavoidable in high magnification DIC because high digital image correlation is usually affected by image distortion due to the spherical geometry of lenses which could introduce large errors in the displacement calculation. Hence, for the mesoscale experiment, distortion correction was done. The process was achieved by following a well-documented approach in [45]. A brief description of the process is stated as follows: First, the speckled specimen was translated in a micrometer assisted linear translation stage to 50μm in both X and Y directions for each step and imaged. A total of 9 steps were performed in both X and Y directions to give a total distance of 450μm for the total translation for both X and Y directions respectively. The image captured during these steps were correlated in Vic 2D software as shown in figure 4.11.

Figure 4.12 shows the variation of horizontal displacement (u-displacement) along with a horizontal line AB. To correct image distortion, a B-spline vector function also known as a warping function was gotten using the data generated from the uncorrected correlated images with a known displacement used for the linear translation. Thereafter, the B-spline vector function is utilized to correct the displacement field. The corrected horizontal displacement is shown in figure 4.12 and an approximate value of 2μm variation was noted from the actual value after correction.

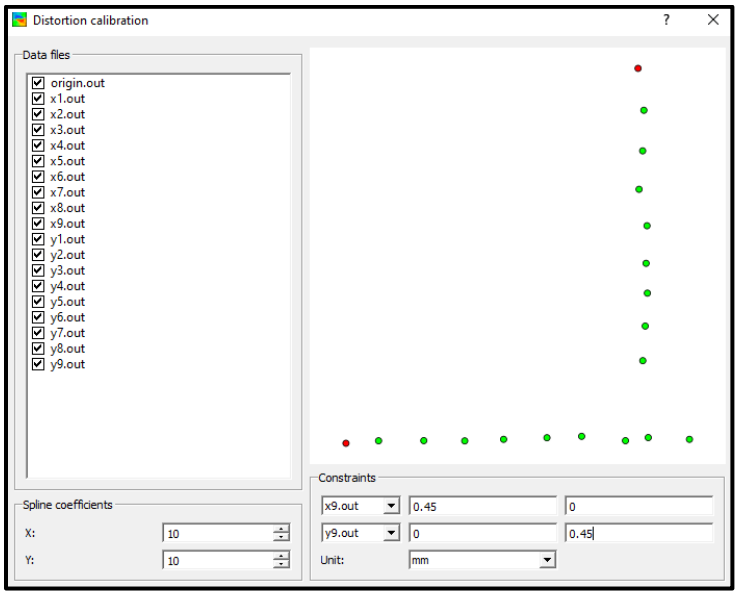

Figure 4.11 diagram showing the analyzed images and plot of the motions

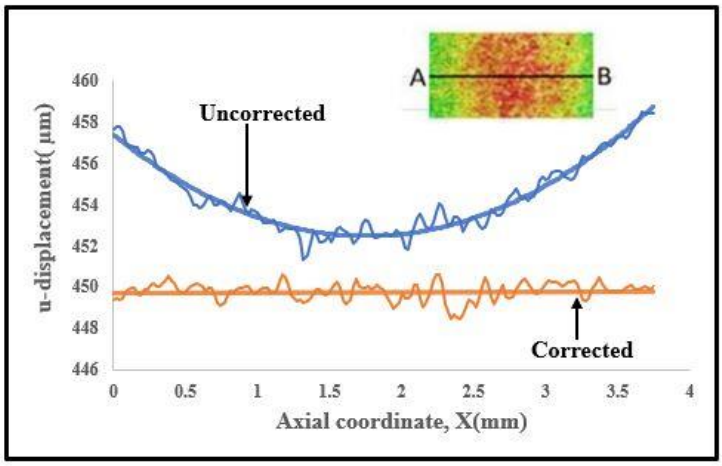

Figure 4.12 Uncorrected and corrected horizontal displacement along a line AB.

The local von mises strain at a global axial strain of 1.41% for coarse, intermediate, fine and superfine crystal size specimen are shown in figure 4.13, It was found out that the local von misses strain field developed during the deformation of PBS for all the crystal size specimens are highly heterogenous. A similar observation was discovered in [10]. The von misses strain field in higher crystal size specimens such as coarse crystal size specimen is highly localized in the polymer rich regions, while the von misses strain field is more dispersed across the specimens with lower crystal size specimen particularly superfine crystal size specimen as seen in figure 4.13.

The main reason for this phenomenon can be explained considering two crystal size specimens: the coarse and superfine crystal size specimens. The coarse crystal size specimen has fewer number of particles as well as greater average spacing between the crystals than the superfine crystal size specimen. The space between the crystals in the coarse specimen is mostly filled with the polymeric binder. Upon application of same external load to both coarse and superfine crystal size specimen, fewer number of force

chain paths would be developed in the coarse crystal size specimen than the superfine crystal size specimen. Consequently, causing stress concentration and strain localization at some areas in the coarse crystal size specimen, particularly the polymer rich regions. This behavior is likely to cause damage to be initiated early in the coarse crystal size specimen as seen earlier where the coarse crystal size specimen started developing fracture as early as 290μs and hence, decreasing the material strength.

On the other hand, superfine crystal size specimen has higher number of crystal-to-crystal contact points than the coarse crystal size specimen. An increase in number of contact points between the crystals would result to a larger contact area across the specimen [46]. Consequently, superfine crystal size specimen would have less strain localization and more uniform strain distribution than the coarse crystal size specimen. Hence, the superfine crystal size specimen is less probable to fracture early (fracturing at about 690μs) because of reduced strain localization, thereby making it have higher strength than the coarse crystal size specimen. A similar explanation can be attributed to intermediate and fine crystal size specimens.

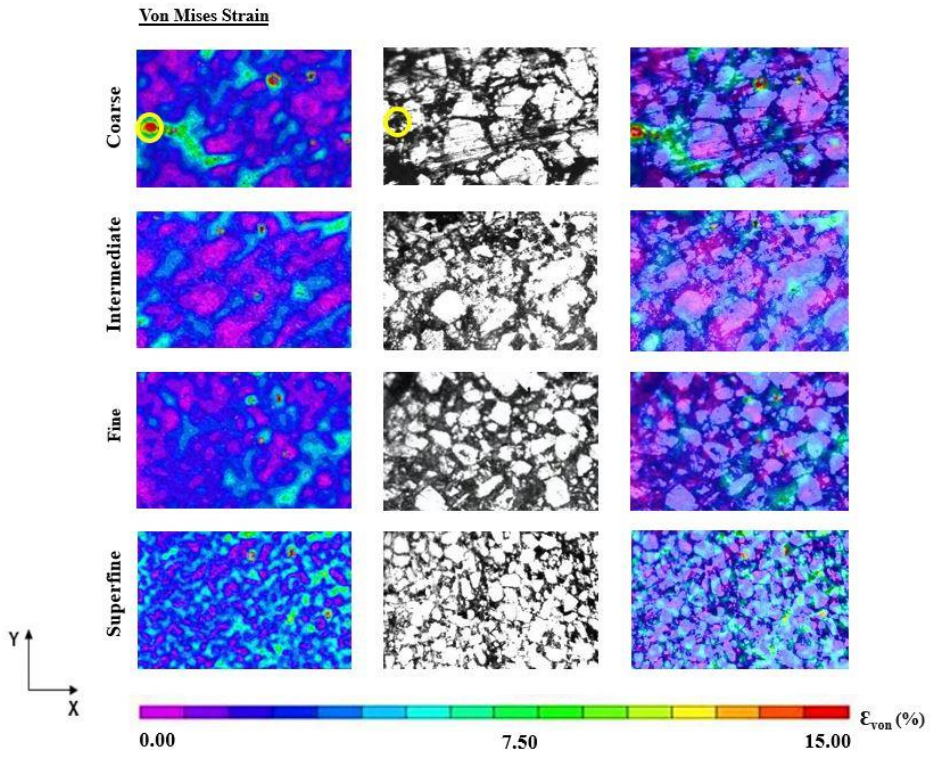

Figure 4.13 The local von Mises strain for coarse, intermediate, fine and superfine crystal size specimens along with the underlying microstructure at a global axial strain of 1.42% (Specific locations are marked)

Figure 4.14 and Figure 4.15 show the local axial and transverse strains for coarse, intermediate, fine and superfine crystal size specimens along with the underlying microstructure respectively. Interestingly, at 1.42% global axial strain, the local axial strain is localized for the coarse crystal size specimen, However, as the crystal size decreases from coarse to superfine crystal size, the local axial strain becomes more evenly distributed especially in superfine crystal size.

The magnitude of the local transverse strain is high, reaching up to 7% for the coarse, and about 2- 4% for the intermediate, fine and superfine crystal size specimens at 1.42% global axial strain. The local transverse strain occurred parallel with each other and at an angle with the loading direction. This striking observation indicates that “shear

band formation" occurred in the specimens as they failed. Like the von Mises strain, the transverse strain is localized in the polymer rich region for the higher crystal size specimens particularly the coarse crystal size specimen and more uniformly distributed across the superfine crystal size specimen, but they are high at the contact point between the crystals in the superfine crystal size. This is the effect of stress concentration at contact points [5] because of a greater number of crystal-to-crystal contacts in the superfine crystal size specimen than in the coarse, intermediate and fine crystal size specimens. In coarse crystal size specimen, the polymer binder carries majority of the load causing strain localization and crack initiation in the polymer binder rich areas.

However, in superfine crystal size specimen, the crystals carry most of the load. This observation could provide more insight as to how the different crystal size specimens could have fractured, coarse, intermediate and fine crystal size specimens could have failed because of crystals debonding from the binder, whereas failure mechanism of the superfine particle size could be dominated by crystal fracture.

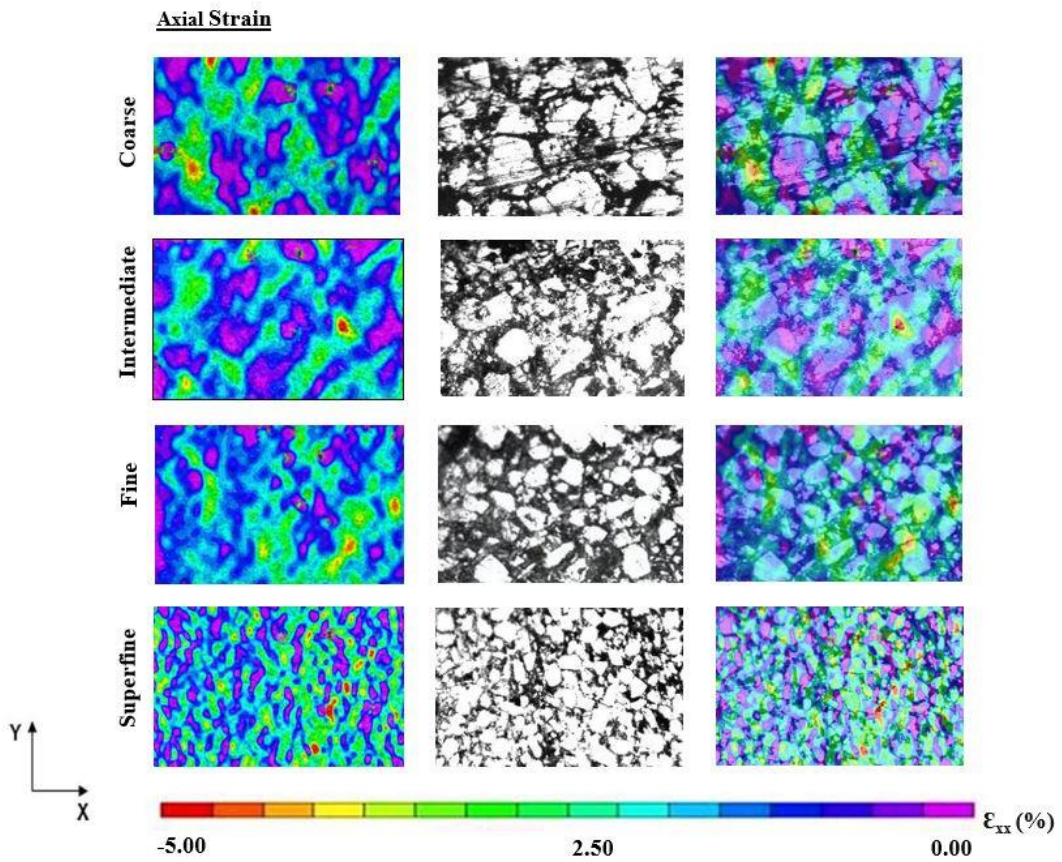

Figure 4.14 The Local axial strain for coarse, intermediate, fine and superfine crystal size specimens along with the underlying microstructure at a global axial strain of 1.42%

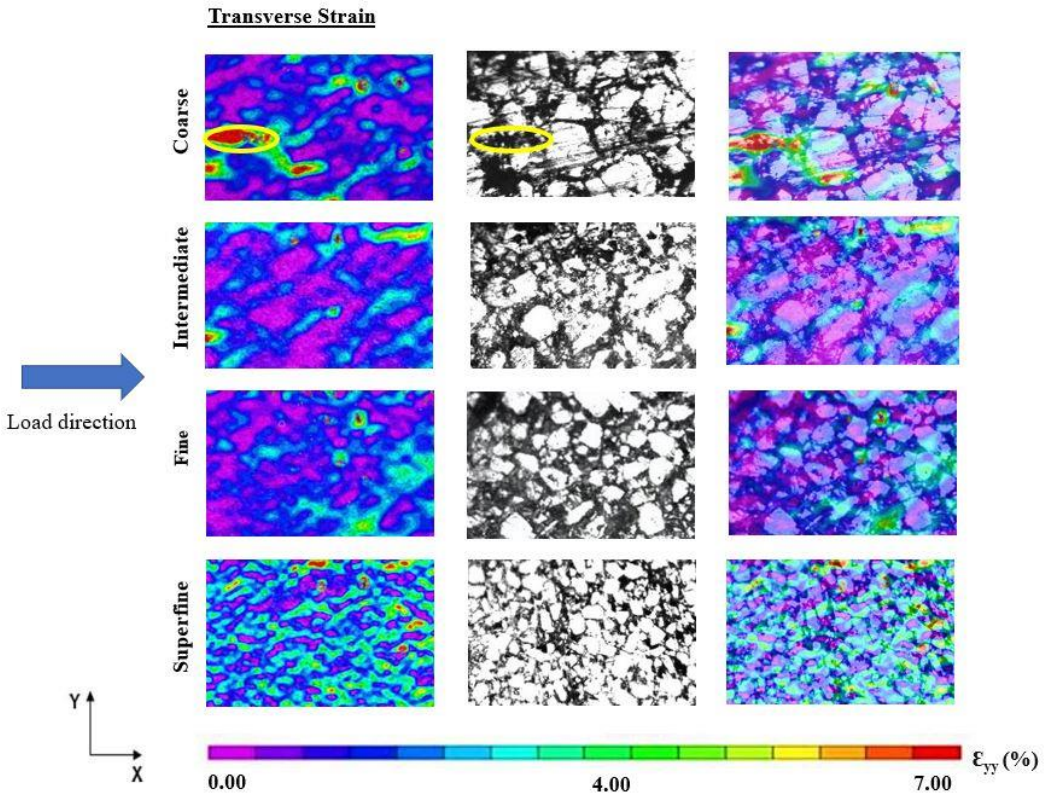

Figure 4.15 The Local transverse at a global axial strain of 1.42% for coarse, intermediate, fine and superfine crystal size specimens along with the underlying microstructure at a global axial strain of 1.42 (Specific locations are marked)

Figure 4.16 (a)-(d) shows the maximum axial, transverse and shear strains at diffent regions where they occur in the microstructure of the coarse, intermediate, fine and superfine particle size respectively. It was observed that the axial, transverse and shear strains are high on the region filled with the polymer binder.

The maximum axial, transverse and shear strains shows a bilinear curve, first, the linear part of the curve starts approximately at t = 0 and remains almost flat upto t=40μs resulting in a nearly 0 slope for all the crystal size specimens. however, the slope increase after t > 40 μs. The magnitude of the transverse strain are high reaching upto 8-12% across all the particle size followed by the axial strain with a value between 4-7% while the shear strains are low. The high transverse, axial and shear strains at time

> 40μs could be an indicator of crack formation in the samples that eventually led to the failure of the materials. It is noted that fracture started initiating at 94 μs for coarse particle size and 98μ for intermediate particle size and the images were not in focus for fine and superfine particle size when fracture initiated.

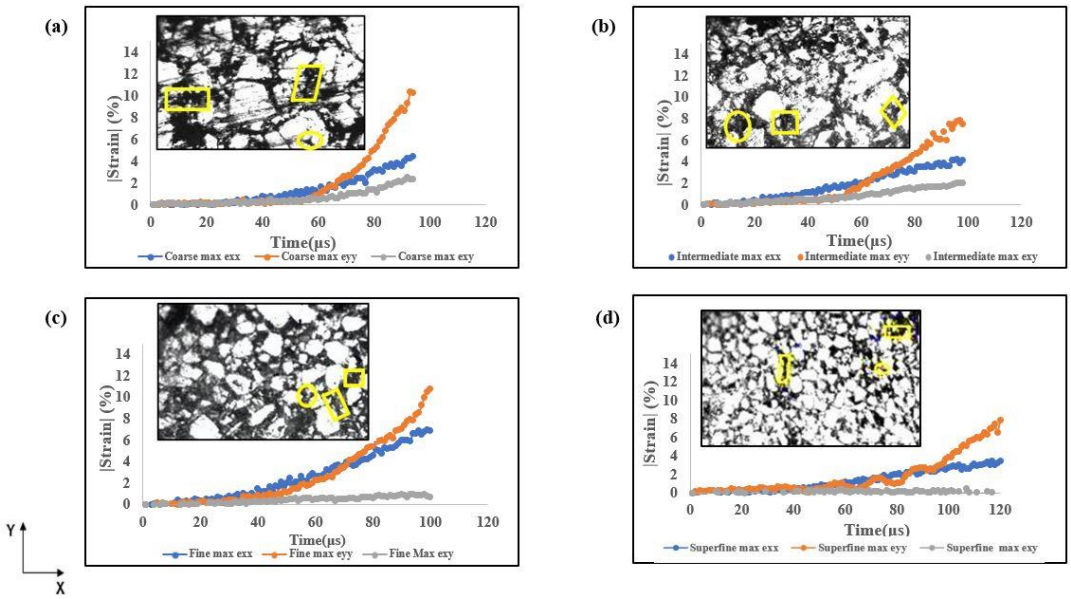

Figure 4.16 The maximum axial, transverse and shear with locations they occur for (a) coarse, (b) intermediate, (c) fine and(d) superfine crystal size specimens. The rectangle, parallelogram and circle shapes are regions in the microstructure where maximum axial, transverse and shear strains occurred respectively

To characterize failure initiation and evolution in all the crystal size of PBS specimens, the volumetric strain as well as the Poisson's ratio is utilized [47].

The Poisson's ratio and volumetric strain are calculated from the average strain obtained from the mesoscale experiments. Three components of strains ε_{xx}, ε_{yy}, ε_{zz} are usually used for the calculation of the volumetric strain [19]. However, since 2D DIC utilized in the experiment can only provide in-plane components of strains ε_{xx} and ε_{yy} the volumetric strain is calculated in this experiment, with only in -plane components ε_{xx}

and ε_{yy} of strain based on the assumption that the lateral strains $\varepsilon_{yy} = \varepsilon_{zz}$ are equal which is a valid assumption for an isotropic material. Hence, the formular utilized to calculate volumetric ratio is $\varepsilon_{vol} = \varepsilon_{xx} + 2 \times \varepsilon_{yy}$.

Figure 4.17 (a)-(d) shows the volumetric strain and average Poisson's ratio for all the crystal size specimens. For coarse crystal size specimen, it is observed that the first 40μs during loading, the average Poisson's ratio is 0.63, and the Poisson's ratio increased to 1.58 between 40 μs to 96 μs which could indicate damage incubation in the material. Further, the average Poisson's ratio for intermediate, fine and superfine crystal size specimens are 0.53, 0.44 and 0.82 respectively for the first 40 μs and the Poisson's ratio increased as time increase for all the crystal size specimens.

Interestingly, the volumetric ratio of all the crystal size specimens is nearly 0 during $t \leq 20\mu s$, loading time . This could indicate the material is incompressible particularly between 0-20μs, however, the intermediate particle size specimen is an exception to this, and the volumetric strain increases nonlinearly with time during loading for all the crystal size specimens.

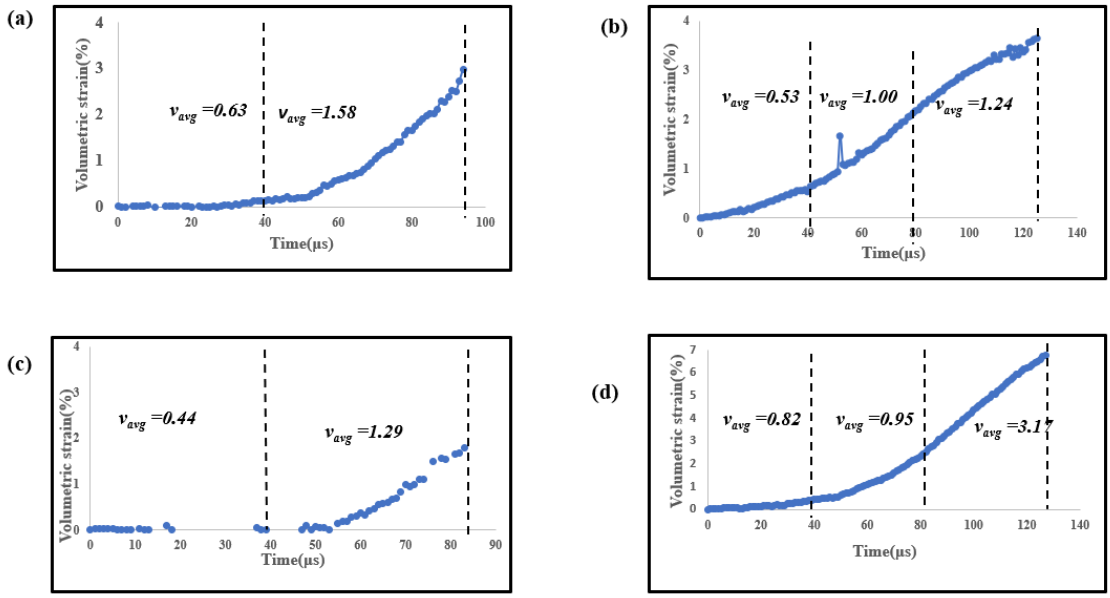

Figure 4.17 The volumetric strain and average Poisson's ratio for (a) coarse, (b) intermediate, (c) fine and (d) superfine crystal size specimens

CHAPTER 5

CONCLUSION

In summary, we studied the effect of crystal size on the deformation behavior of polymer bonded sugar under dynamic load . Four different crystal sizes of PBS : coarse, intermediate, fine and superfine crystals corresponding to crystal sizes of 600-850 μm, 425-600 μm, 212-425 μm, and 100-212 μm, respectively are used for the study. High speed camera along high magnification tube is employed to study the local and global deformation behavior of the different crystal sizes.

The macroscale experiment shows that as the crystal size increase from superfine crystal size to coarse crystal size, the ultimate compressive stress of the PBS decreases while the mesoscale experiment shows that the local von misses strain field of PBS for all the crystal size specimens are highly heterogenous, the von misses strain field in higher crystal size specimens such as coarse crystal size specimen is highly localized, occurring in the polymer rich regions, however, becomes evenly distributed as the crystal size decreases.

Further, the local axial and transverse strain are highly localized for the higher crystal size specimen (coarse particle size) and becomes more evenly distributed as the crystal size decreases. The polymer binder carries majority of the load in higher crystal size specimen (coarse crystal size) causing strain localization and crack initiation in the polymer binder rich areas. However, the crystals carry most of the load in the lower crystal size specimens (superfine crystal size).

5.1 FUTURE WORK

The following future work is suggested:

(1) Investigate the effect of strain rate on the different crystal sizes of polymer bonded sugar.

(2) Investigate the surface modification of the different particle size on the deformation mechanics of PBS.

(3) Investigate the effect of different polymeric binders on deformation mechanics of PBS.

REFERENCES

[1] Goldrein HT, Rae PJ, Palmer SJP, Lewis AL (2001) Ageing Effects on the Mechanical Properties of a Polymer Bonded Explosive. In: Mallinson L.G. (eds) Ageing Studies and Lifetime Extension of Materials. Springer Boston MA.

[2] Youcai X, Xiangdong X , Yanyi et al. (2021) Mechanical behavior of a typical polymer bonded explosive under compressive loads. Journal of Energetic Materials.

[3] Catzin, Carlos A (2016) Manufacturing and characterization of energetic materials. ETD Collection for University of Texas, El Paso. AAI10118239.

[4] Ravindran S, Tessema A, Kidane A (2016) Local Deformation and Failure Mechanisms of Polymer Bonded Energetic Materials Subjected to High Strain Rate Loading. J. dynamic behavior mater. 2, 146–156.

[5] Ravindran S, Gupta V, Tessema A et al. (2019) Effect of Particle Mass Fraction on the Multiscale Dynamic Failure Behavior of Particulate Polymer Composites. Exp Mech 59, 599–609.

[6] Palmer S J P, Field J E, Huntley J M (1993) Deformation strengths and strains to failure of polymer bonded explosives Proc R Soc Lond A440399 419.

[7] Siviour CR, Laity PR, Proud et al (2008) High strain rate properties of a polymer-bonded sugar their dependence on applied and internal constraints. Proc R Soc a Math. Phys Eng Sci 464. pp 1229–1255.

[8] Yuliang L, Binbin X, Rong C, et al (2014) Dynamic Mechanical Properties and Constitutive Relation of an Aluminized Polymer Bonded Explosive at Low Temperatures. Shock and Vibration vol. 2014 Article ID 918103, 6 pages.

[9] Li S, Xiao J (2021) Molecular Dynamics Simulations for Effects of Fluoropolymer Binder Content in CL-20/TNT Based Polymer-Bonded Explosives. Molecules 26: 4876.

[10] Ravindran S M (2018) Multiscale Deformation and Failure Behavior of Polymer Bonded Explosives Subjected to High-Rate Loading. Doctoral Dissertation University of South Carolina. Retrieved from

[11] Roessig KM (2002) Mesoscale mechanics of plastic bonded explosives. In: AIP conference proceedings. IOP INSTITUTE OF PHYSICS PUBLISHING LTD, pp 973–978

[12] Field JE (1992) Hot spot ignition mechanisms for explosives. Acc Chem Res 25:489–496

[13] Kraus, H., (1980) Creep Analysis, John Wiley, New York

[14] Siviour CR, Gifford MJ, Walley SM et al (2004) Particle size effects on the mechanical properties of a polymer bonded explosive. Journal of Materials Science 39, pp 1255–1258.

[15] Xiaochuan L, Xulong X, Chunyu B (2019) Dynamic response and failure mechanism of Ti-6AL-4 V hi-lock bolts under combined tensile-shear loading Int. J. Impact Eng., 31 pp. 140-151.

[16] Joseph R S (2019) Design of a split Hopkinson pressure bar facility for dynamic material characterization master's thesis, Rutgers, the State University of new Jersey

[17] Nathan J M (2010) Characterization of dynamic and static mechanical behavior of polyetherimide master's thesis University of Central Florida Orlando, Florida.

[18] Parab N D, Roberts Z A, et al. (2016) High speed X-ray phase contrast imaging of energetic composites under dynamic compression Appl. Phys. Lett., 109 Article 131903

[19] Ravindran S, Tessema A, Kidane A, (2017) Multiscale damage evolution in polymer bonded sugar under dynamic loading, Mechanics of Materials, Vol. 114, 97-106, 201.

[20] Siviour C R, Williamson D M, Grantham S G,. Palmer S J P, Proud, *W G* and Field J E (2004) Split Hopkinson Bar Measurements of PBXS, AIP Conference Proceedings 706, 804-807.

[21] Zhou Z , Chen P, Duan Z, Huang F(2012) Study on Fracture Behavior of a Polymer-Bonded Explosive Simulant Subjected to Uniaxial Compression Using Digital Image Correlation Method Strain ISSN: 0039-2103 Volume 48 Issue 4 Page Numbers 326-332.

[22] Strain gage Wikipedia at: https://en.wikipedia.org/wiki/Strain_gauge

[23] Tokyo Measuring Instrument Lab article on strain gage retrieved from: https://tml.jp/e/knowledge/strain_gauge/about.html

[24] Begonia, Mark T et al. (2015) Non-contact strain measurement in the mouse forearm loading model using digital image correlation (DIC). *Bone* vol. 81: 593-601.

[25] Peters W H, Ranson W F, Sutton M. A. et al. (1983) Application of digital correlation methods to rigid body mechanics. Opt. Eng. 22, 738–742

[26] Keiichiro T, Itoh Y, Yoshinobu S (2010) A constitutive model of particulate-reinforced composites taking account of particle size effects and damage evolution, Composites Part A: Applied Science and Manufacturing, Volume 41, Issue 2, Pages 313-321, ISSN 1359-835X.

[27] Sankaye S S (2011) Dynamic testing to determine some mechanical properties of aluminum, copper, and dry Eglin sand using split Hopkinson pressure bar (SHPB), high speed photography and digital image correlation (DIC) Master's thesis Oklahoma State University.

[28] Kumar KR, Mohanasundaram KM, et al. (2012) Effect of particle size on mechanical properties and tribological behavior of aluminum/fly ash composites. Science and Engineering of Composite Materials, vol 19 no 3, pp 247-253.

[29] Shao-Yun F, Xi-Qiao F, Bernd L, Yiu-Wing M (2008) Effects of particle size, particle/matrix interface adhesion and particle loading on mechanical properties of particulate–polymer composites. Composites Part B: Engineering Volume 39 Issue 6 pp 933-961 ISSN 1359-8368.

[30] Matthew J H, Caitlin SW, et al. (2021) Composite binder processing and particle size effects on mechanical properties of non-hazardous high explosive surrogates. Powder Technology Volume 391 pp 442-449, ISSN 0032-5910.

[31] Sheffield S, Gustavsen R, Alcon R (1998) Porous hmx initiation studies—sugar as an inert simulant. AIP Conference Proceedings 429, American Institute of Physics pp. 575–578.

[32] Thompson G, Brown B, Olinger et al (2010) The effects of TATB ratchet growth on PBX 9502 Propellants. Explos. Pyrotech. 35 pp507–513

[33] Kezhen L V, et al. (2021) The densification and mechanical behaviors of large-diameter polymer-bonded explosives processed by ultrasonic-assisted powder compaction, Materials & Design, Volume 207, 2021, 109872, ISSN 0264-1275

[34] Balzer J E, Siviour C R, Walley S M and Field J E (2004) Behavior of ammonium perchlorate–based propellants and a polymer–bonded explosive under impact loading Proc. R. Soc. Lond. A.460781–806.

[35] Drodge D R and Williamson D M (2016) Understanding damage in polymer-bonded explosive composites Journal of Materials Science, vol. 51, no. 2, pp. 668

[36] Merran A (2006) Polyurethane Binder Systems for Polymer Bonded Explosive Daniel Weapons Systems Division Defence Science and Technology Organisation DSTO-GD-0492.

[37] Technical report of Hydroxyl terminated polybutadiene retrieved from https://www.crayvalley.com/docs/technical-paper/hydroxyl-terminated-polybutadiene-resins-and-derivatives.pdf

[38] Parod RJ (2014) Toluene Diisocyanate, Editor(s): Philip Wexler, Encyclopedia of Toxicology (Third Edition), Academic Press Pages 599-603, ISBN 9780123864550,

[39] Allen D G, plasticizers,(2000) Applied polymer science: pages 157-175, ISBN 9780080434179.

[40] Liu C (2005) On the minimum size of representative volume element: an experimental investigation. Exp Mech 45:238–243

[41] Asadi M (2006) Beet-sugar handbook. Wiley, Hoboken

[42] Sutton MA, Orteu JJ, Schreier H. (2009) Image Correlation for Shape, Motion and Deformation Measurements: Basic Concepts, Theory and Applications. Springer Science & Business Media; ISBN: 978-0-387-78746-6.

[43] Zhao H, Gary G, Klepaczko JR, (1997) On the use of a viscoelastic split Hopkinson pressure bar. Int J Impact Eng 19:319–330.

[44] Signal Conditioning Amplifier 2310A instruction Manual (2004) Vishay Micro-Measurement

[45] Schreier H W, Garcia D, Sutton M A (2004) Advances in light microscope stereo vision. Exp. Mech. 44, pp 278–288.

[46] Rumchik CG, Jordan JL, Elert M, et al. (2007) Effect of aluminum particle size on the high strain rate properties of pressed aluminized explosives. AIP Conf Proc 955 795–8.

[47] Lazzeri A, Thio YS, Cohen R E (2004) Volume strain measurements on CaCO3/polypropylene particulate composites: the effect of particle size. J Appl Polym Sci 91, pp 925–935.